Received: 3 June 2023 | Revised: 14 August 2023 | Accepted: 25 August 2023

DOI: 10.1111/jace.19469

Journal of the American Ceramic Society

RESEARCH ARTICLE

Effect of resting time on rheological properties of glass bead suspensions: Depletion and bridging force among particles

Yanliang Ji[1] | **Simon Becker**[2] | **Zichen Lu**[3] | **Alexander Mezhov**[4] | **Regine von Klitzing**[2] | **Schmidt Wolfram**[4] | **Dietmar Stephan**[1]

[1]Department of Civil Engineering, Technische Universität Berlin, Berlin, Germany

[2]Division of Soft Matter at Interfaces, Department of Physics, Technische Universität Darmstadt, Darmstadt, Germany

[3]Key Laboratory of Advanced Civil Engineering Materials, Ministry of Education, Tongji University, Shanghai, China

[4]Division of Technology of Construction Materials, Bundesanstalt für Materialforschung und Prüfung (BAM), Berlin, Germany

Correspondence
Yanliang Ji and Dietmar Stephan, Department of Civil Engineering, Technische Universität Berlin, Berlin 13355, Germany.
Email: ji@tu-berlin.de and stephan@tu-berlin.de

Zichen Lu, Key Laboratory of Advanced Civil Engineering Materials, Ministry of Education, Tongji University, Shanghai 201804, China.
Email: luzc@tongji.edu.cn

Funding information
German Research Foundation (DFG), Grant/Award Number: 387092747

Abstract

The effect of resting time on the rheological properties of cement suspensions is generally explained by early formed structure and overconsumption of polycarboxylate superplasticizers (PCEs). In this paper, we propose that the influence of resting time on the rheological properties is closely related to size variation of non-absorbed PCE. To identify this, glass bead suspensions were prepared with various amounts of PCE and ionic solution, and their rheological properties were evaluated at various times. We found that the yield stress increases with time at higher PCE concentrations and higher ionic strength solutions. Adsorbed PCE during resting tends to bridge the particles rather than disperse them. In addition, it was found that hydrodynamic radius of PCE increased with resting time, and depletion forces resulting from non-absorbed PCE size changes correlate well with the increased yield stress.

KEYWORDS
depletion force, ionic strength, PCE, rheology, resting time

1 | INTRODUCTION

Rheological properties are crucial to fresh cementitious materials since they affect the mixing, pumping, and casting in the fresh stage and even the long-term mechanical strength and durability.[1] In practical engineering, fresh cementitious materials (i.e., cement paste, mortar, and concrete) may have to wait for some time before they become available at the job site, depending on their transportation distance and speed.[1–3] For a particular type of concrete, such as 3D printing or precast concrete, the tailored rheological property is often needed after various resting times until the following procedures are ready.[4,5] Therefore, it raises general but practical concerns about how the resting time influences the rheological properties of cementitious materials and the reasons for this.

One of the apparent mechanisms for changing rheological properties with time is the development of the internal structure during the induction period of hydration. Early-age hydration at various resting times is characterized by the consumption of free water in the cement suspension[5] and the formation of a denser structure from cement grains and hydrates (i.e., ettringite or portlandite),[6,7] leading to the loss of workability or flowability. To alleviate the detrimental impact of hydration on rheology, measures such as reducing cement amount, using low reactive supplementary cementitious materials (i.e., slag or fly ash), or adding various retarders[8–10] are considered in the concrete mix design to suppress the hydration and achieve longer but sufficient workability. Another mechanism for the loss of workability due to the resting time is the loss of efficiency of the dispersion agent (i.e., superplasticizers) resulting from hydrate coverage or over-adsorption by the small hydrates formed during the resting time.[9,11] Polycarboxylate superplasticizers (PCEs) are comb-shaped polymers with an anionic backbone and several non-ionic side chains,[8,9] and are widely used in cement concrete. It has been known that the hydrates may grow on or cover the adsorbed PCE molecules on the surface of cement grains, reducing electrostatic repulsion and steric hindrance effects as a function of time.[12] Regarding this mechanism, the PCEs with a longer side chain but lower charge density (less carboxylate groups)[9,13,14] and PCEs with hydroxy alkyl side chains[15] at high dosages are more effective in maintaining the slump retention of concrete, as a certain amount of free PCEs in pore solution can gradually adsorb on cement particles and become functional over time.

It is noted that the above mechanisms have provided us with a fundamental understanding of the effect of resting time on rheology, although many research questions remain. For instance, the movement of solid particles over time would be inseparable from the impact of the aqueous phase, in which different species of ions and non-absorbed polymers (i.e., PCE) are present.[16] The existence of ions and non-absorbed polymers and their interactions in the aqueous phase would lead to multiple effects on the system of a cement-based material with resting time. Individually, cations such as K^+ or Ca^{2+} released from the hydration process can interact with water molecules and form more hydrogen bonds among water molecules, creating a closer distance among molecules in pore solutions.[17,18] As a result, the viscosity of the aqueous phase, in theory, would be increased to a certain degree,[19] which leads to the higher viscosity of cement suspension, according to Einstein's equation in theory.[20,21] Besides, the increase in ionic strength in the early stage in pore solution can also implement the shielding effect and result in a shorter range of Debye length,[22,23] which undermines the possible electrostatic force among particles and then increases the yield stress of a system.

In addition, the depletion force generated by non-absorbed polymers would contribute to the formation of flocculants if the distance is close enough.[16,24] These non-absorbed PCE polymers may interact with ions by the complexation, which may change the morphology or conformation (i.e., size) of the polymers and possibly lead to impacts on rheology over time.[25,26] However, in practice, the above mechanisms are not easily identified due to many factors (i.e., hydrate formation, ions released from cement, and water consumption), which change with the hydration process over time, etc.

In this study, well-purified glass beads (GB) were used as a modeling system to mimic cement suspension, which allows us to focus on the interaction between ions and PCE and their impact on rheological properties over time. The shear yield stress and oscillation strain sweep were jointly used to evaluate the rheological performance. With the three-component GB-ionic solution–PCE system, influencing factors of PCE in the different types of solutions, different dosages of PCE in artificial pore solutions (APs), and PCE in various types of ionic strength solutions (potassium chloride [KCl] and calcium chloride [$CaCl_2$]) on the rheological behavior at various resting times were investigated at first. Using zeta potential and total organic carbon (TOC) measurements, variations in surface electrical properties and PCE adsorption over time were investigated. Using the dynamic light scattering (DLS) measurements of the relative hydrodynamic radius of the PCE in ionic solutions, the bridging effect and depletion force resulting from PCE size change and their relations to the yield stress are discussed.

2 | MATERIALS AND EXPERIMENTAL SETUP

2.1 | Materials

2.1.1 | Glass beads

The GBs used in this study were purchased from Sigmund Lindner GmbH (Germany), and the main chemical composition was SiO_2 (72.3 wt.%), Na_2O (13.3 wt.%), CaO (8.9 wt.%), MgO (4.0 wt.%), and residue (1.5 wt.%), as measured in a previous study.[27] It should also be mentioned that the pore solution extracted from GB suspension (the solid-to-water ratio is 1:20) contains ions such as Na^+, K^+, and Ca^{2+}, which are released from the GBs. These ions can interfere with the rheological measurement and characterization (i.e., zeta potential), therefore, they need to be removed. In this study, the GBs are purified by a series of cleaning processes, including a magnetically stirred process, long-term (48 h) sedimentation and grinding. After sedimentation, the wet GB paste was dried for 7 days in a

TABLE 1 Elemental concentration of a solution prepared with the glass beads, before and after the purification (solid-to-water ratio is 1:20).

Element	Before purification (mmol/L)	After purification (mmol/L)
Al	0.00456	0.00108
Ca	0.518	0.127
K	0.0287	0.0081
Na	33.859	0.0741
S	1.930	0.003
Si	2.903	0.270

vacuum dryer. The crushed GB particles were then loaded into a jar with four agate balls and ground for 24 h on a rolling device, in which the speed of rotation can be as low as 0.5 rps. The inductively coupled plasma (ICP) results before and after purification are listed in Table 1, and the ions released were determined by an inductively coupled plasma and atomic emission spectrometry (ICP-AES Horiba Ultima 2000).

It can be seen that all element concentrations were drastically reduced after the purification described above, that is, the element of Na in solution was minimized from 33.859 to 0.0741 mmol/L, which eased the impact on rheological properties from the GBs themselves. The morphology of the GBs before and after the purification process is shown in Figure 1. It can be seen that the purification process removes smaller particles from the GBs, which leads to almost perfect spherical-shaped particles with clean surfaces for the rheological study. The particle size distribution of the purified GBs used in our study is plotted in Figure 2. The mean volume particle diameter of GBs measured by laser diffraction scattering (Malvern Mastersizer S) dispersed in water is 9.13 μm. The specific surface area and density of the GBs were 4060 cm^2/g (Blaine) and 2.2 kg/m^3, respectively.

2.1.2 | Ionic solutions and admixtures

In this study, four types of solutions were prepared: deionized water (DI water), APs, KCl solution, and $CaCl_2$ solution. The recipe for the APs is taken from Refs.[28, 29] Accordingly, the potassium hydroxide (KOH = 7.12 g), sodium sulfate (Na_2SO_4 = 6.96 g), potassium sulfate (K_2SO_4 = 4.76 g), and calcium sulfate decahydrate ($Ca_2SO_4 \cdot 2H_2O$ = 1.72 g) with a purity of 99.8 wt.% were dissolved into 1000 mL DI water for the APs. The conductivity and pH of the APs are 39 mS/cm and 12.4, respectively. Its ionic strength is around 386 mM. The KCl and $CaCl_2$ solutions had ionic strengths of 0, 3, 60, and 180 mM, and the pH was adjusted by sodium hydroxide to a value of 12 ± 0.2.

PCE is provided by BASF, which has a solid content of 23.5 wt.%. M_w and M_n for the PCE are 28 090 and 11 770 g/mol, respectively. Detailed information regarding the PCE molecule structure and chemical compositions, as well as related experiments about the dispersing effect of the PCE on cement, can be found elsewhere.[30]

2.2 | Sample preparation

The GB suspensions were prepared at a solution-to-glass bead ratio of 0.26. The low glass ratio selected in this study prevents sample segregation and bleeding. In the case of DI water, with or without 0.20% of PCE by GB weight was compared. For the APs, the PCE dosage from 0 to 0.40 wt.% of GBs was changed for the sample preparation. For KCl and $CaCl_2$ solutions, the PCE dosage is fixed at 0.20 wt.% and the ionic strength of the solution is changed. The material design for the GB suspension is shown in Table 2.

The sample was first homogenized at 280 rpm for 1 min, then mixed at 310 rpm for another minute using a hand mixer (HM-753BG, Qilive). The GB suspension was then used for the first measurement (i.e., rheology, zeta potential, or adsorption). Afterward, the beaker with GBs was

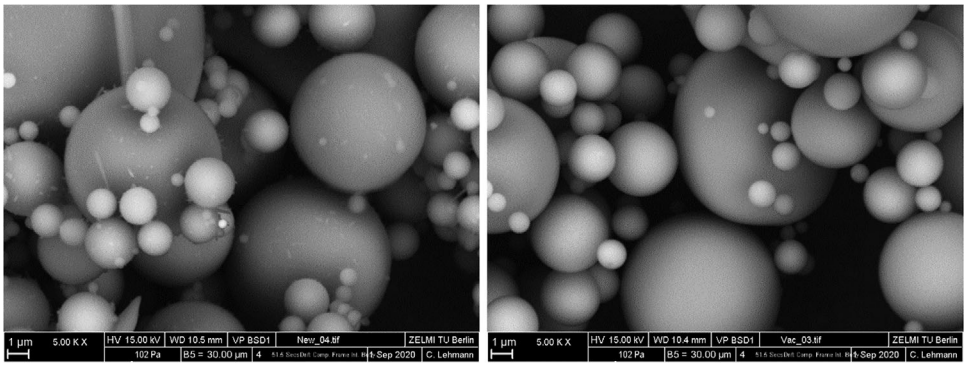

FIGURE 1 Scanning electron microscopy images of the glass beads before (left) and after (right) the purification process.

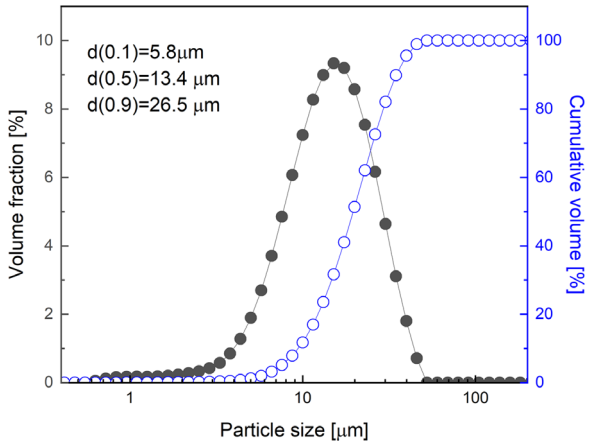

FIGURE 2 Particle size distribution of the glass beads used in this study.

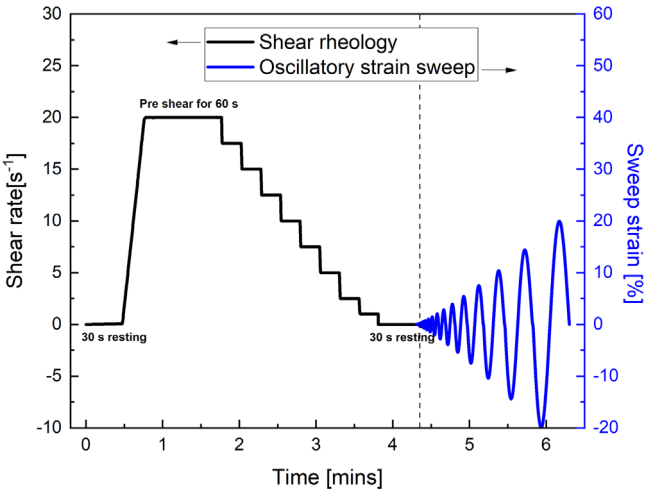

FIGURE 3 Schematic of steady shear rheology and oscillatory strain sweep measurement.

sealed with plastic paper during the resting period to keep it from moisture evaporation. To reduce the sedimentation impacts on rheological properties, the suspension was remixed for 30 s at 280 rpm at the resting times of 30, 60, and 120 min before the measurements.

2.3 | Experimental setup

2.3.1 | Rheological measurements

The rheometer used in this study was a HAAKE RheoStress 600 (Thermo Electron Corporation). In this study, we chose a bob in cup geometry (d_0 = 20 mm and d_a = 21.7 mm) for the rheological measurement, which was carried out at 22°C. Two modes of rheological measurements, rotational shear test and sweep oscillation, are applied to the prepared suspension. A schematic of steady shear rheology and oscillatory strain sweep measurement is shown in Figure 3. The shear rate increased from 0 to 20 s^{-1} and then kept at a shearing rate of 20 s^{-1} for 60 s. Afterward, the shear rate gradually decreased to 1.0 s^{-1} within 3 min.

After that, a sweep oscillation measurement was conducted. The sweep frequency was kept at a constant frequency of 1.0 Hz, and the shear strain logarithmically swept from 10^{-4}% to 20% during the measurement. The oscillatory strain sweep test can obtain the storage

TABLE 2 Material design for the glass bead suspension.

Sample	Glass beads (g)	PCE (g)	DI water (g)	Artificial pore solution (g)	KCl solutions (g)	$CaCl_2$ solutions (g)
DI water	100	–	26	–	–	–
DI water–PCE0.2	100	0.2	26	–	–	–
APs–PCE0.0	100	–	–	26	–	–
APs–PCE0.1	100	0.1	–	26	–	–
APs–PCE0.2	100	0.2	–	26	–	–
APs–PCE0.4	100	0.4	–	26	–	–
KCl–0 mM –PCE0.2	100	0.2	–	–	26 (IS = 0 mM)	–
KCl–3 mM–PCE0.2	100	0.2	–	–	26 (IS = 3 mM)	–
KCl–60 mM–PCE0.2	100	0.2	–	–	26 (IS = 60 mM)	–
KCl–180 mM–PCE0.2	100	0.2	–	–	26 (IS = 180 mM)	–
$CaCl_2$–0 mM–PCE0.2	100	0.2	–	–	–	26 (IS = 0 mM)
$CaCl_2$–3 mM–PCE0.2	100	0.2	–	–	–	26 (IS = 3 mM)
$CaCl_2$–60 mM–PCE0.2	100	0.2	–	–	–	26 (IS = 60 mM)
$CaCl_2$–180 mM–PCE0.2	100	0.2	–	–	–	26 (IS = 180 mM)

Abbreviations: APs, artificial pore solutions; DI water, deionized water; IS, ionic strength; PCE, polycarboxylate superplasticizer.

modulus (G') and loss modulus (G''). The storage modulus (G') and loss modulus (G'') are related to the energy stored and dissipated in each measuring cycle, respectively,[31] which jointly can characterize the viscoelastic behavior of the GB suspension at various resting times.

2.3.2 | Zeta potential

The zeta potential device (DT-310, Dispersion Technology) used in this study is based on the electroacoustic behavior among particles in the sample. In this study, liquid density was considered according to the concentration and composition of salts and then used to calculate zeta potential. With an identical process (described in Section 2.2), the sample was prepared and loaded, and then the GB suspensions at various resting times of 0, 60, and 120 min were measured. The temperature was kept constant at 22°C during the measurement. Each measurement was repeated three times, and the average value for the zeta potential was calculated.

2.3.3 | Adsorption

The sample at the resting times of 0, 60, and 120 min was centrifuged at 3000 rpm for 5 min, and then the supernatant liquid was filtered by a 0.45 μm membrane. After being diluted 20 times with DI water, the prepared solution was then measured using a TOC (TNM-L, Shimadzu) analyzer, which allowed us to calculate the amount of PCE in the solution and the adsorbed amount on the surface of the GBs.

2.3.4 | Dynamic light scattering

The hydrodynamic diameter of PCE in solution at different times was measured with a DLS instrument (Malvern Instruments Ltd.). The detector position at 173° was selected as the optical arrangement. For the measurement, the PCE and solution were mixed using a hand mixer at 0, 60, and 120 min. Then, impurities (i.e., large particles), possibly from synthesis, transportation, or storage, in the PCE-containing solution were removed using a 1.0 μm membrane with a syringe. We repeated each measurement five times, and the average value was taken as the hydrodynamic diameter. The size of a particle is calculated based on the translational diffusion coefficient by using the Stokes-Einstein equation (Equation 1)[32,33]:

$$d_H = \frac{kT}{3\pi\eta D} \quad (1)$$

$$d_R(t) = \frac{d_H(t)}{d_H(0)} \quad (2)$$

where d_H is the hydrodynamic diameter, D is the translational diffusion coefficient, k is Boltzmann's constant, and η is the fluid viscosity. The diameter measured by the DLS is the diameter of a sphere with the same translational diffusion coefficient as the particle. In this study, solutions with different ionic strengths are used, which can affect the PCE polymer diffusion speed by changing the thickness of the electric double layers.[33] Therefore, the DLS measurement cannot obtain the absolute value of the hydrodynamic diameter when ionic strength is changed in the solution. Therefore, instead, relative hydrodynamic diameter, $d_R(t)$, the ratio between values measured at each observed time step(t) and 0 min as described in Equation (2) is taken to evaluate the PCE size as a function of time.

3 | EXPERIMENTAL RESULTS

3.1 | Rheological properties of glass bead suspension

3.1.1 | Yield stress as a function of resting time

The Herschel-Bulkley model was applied to fit the data from 20 to 2.5 s^{-1} to calculate the dynamic yield stress (τ_0). The results of yield stress as a function of time for GB suspensions are plotted in Figure 4, that is, Figure 4A shows the sample prepared without or with PCE (0.2 wt.%) in which APs and DI water are varied, and Figure 4B shows the sample prepared by APs in which the PCE dosages varied from 0% to 0.40% by GB weight.

In DI water with or without PCE, the yield stress of the sample keeps constant over resting time, and the sample with DI water and PCE has a higher yield stress than that of the sample without PCE. For the GB suspension prepared with APs, the yield stress decreases and then increases to a certain degree. In the case of GB suspension mixed with the artificial solution and PCE, the yield stress at 0 min is lower than that of GB suspension with the APs but without PCE. In addition, a clear yield stress increase trend as a function of resting time was observed. The values at 120 min with PCE are even higher than those of the GB suspension with APs but without PCE. In Figure 4B, the yield stress of GB suspension is smaller at 0 min when PCE is added, and over the dosage of 0.20% by GB weight, the yield stress increased with PCE dosage at 0 min. Another observation is that the yield stress increased as a function

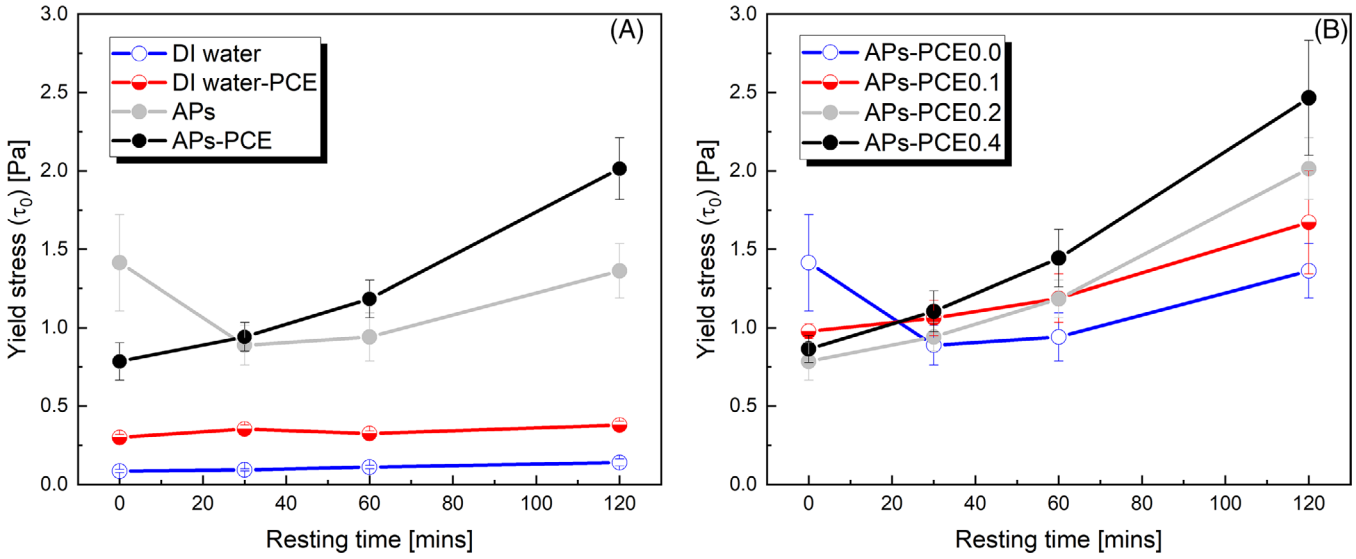

FIGURE 4 Yield stress as a function of time for glass bead suspensions: (A) prepared without or with polycarboxylate superplasticizer (PCE) (0.20 wt.%) in which deionized (DI) water or artificial pore solution (APs) is used; (B) prepared by APs in which the PCE dosage is varied from 0 to 0.40% by glass bead weight.

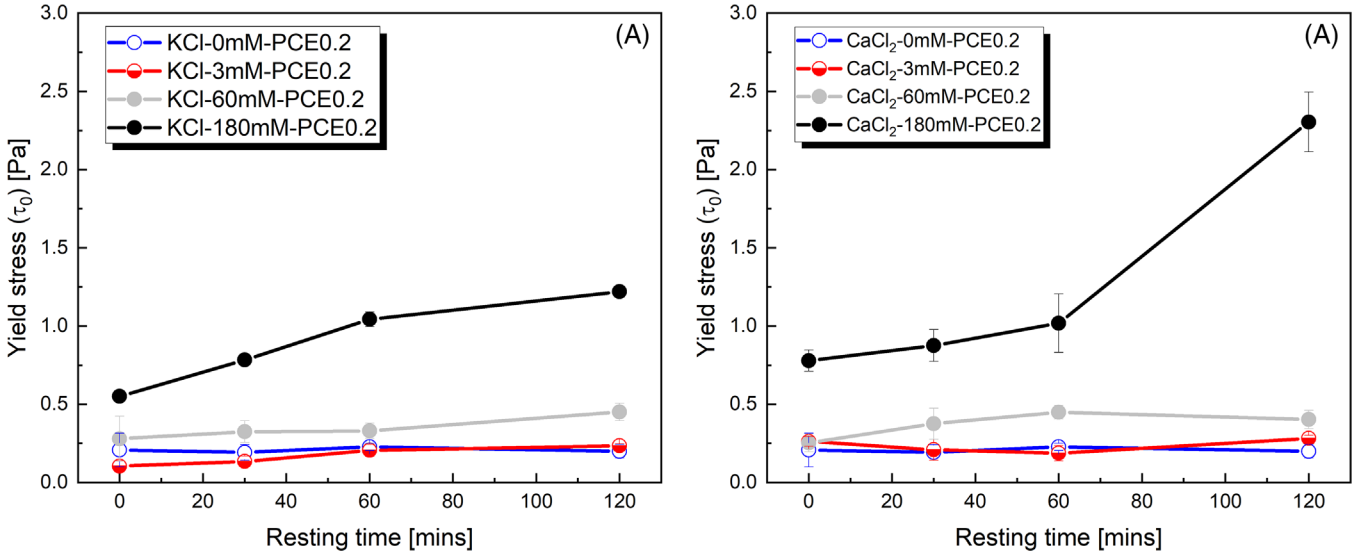

FIGURE 5 Yield stress as a function of time for glass bead suspension prepared with 0.20% polycarboxylate superplasticizer (PCE) in which ionic strength of KCl (A) and $CaCl_2$ (B) ranges from 0 to 180 mM.

of resting time, and the increased degree of yield stress over time is enhanced when more PCE is used in the sample.

The yield stress as a function of time in GB suspension prepared with 0.2% PCE in which ionic strengths of KCl and $CaCl_2$ vary from 0 to 180 mM is shown in Figure 5A,B, respectively. In general, the higher ionic strength can result in higher yield stress, as shown in Figure 5. Besides, at a low ionic strength (0 and 3 mM for KCl and $CaCl_2$), the yield stress is kept constant over time, while the yield stress is found to increase as a function of resting time when the ionic strength is higher than 60 mM. At an ionic strength of 180 mM, the yield stress for GB suspension prepared by 0.20% PCE with $CaCl_2$ solution is higher than that of the sample prepared with KCl solution.

3.1.2 | Sweep oscillation at different resting times

The results of sweep oscillation measurement, storage modulus (G'), and loss modulus (G'') modulus as a func-

tion of sweep oscillation strain of GB suspension prepared with different ionic solutions and PCEs at 0, 60, and 120 min are compared in Figure 6.

The results shown in Figure 6 indicate that, generally, the storage modulus (G') and loss modulus (G'') of GB suspension gradually decrease as a function of strain. For the DI water and 0.20% dosage of PCE-made sample, both the storage modulus (G') and loss modulus (G'') at 0, 60, and 120 min overlap, which suggests that the rheological properties of GB suspension are not changed.

As shown in Figure 6B–D, the resting time has an apparent influence on the storage modulus (G') and loss modulus (G'') curves over oscillation strain (curves shifted to the right) when PCE and APs are used. In general, a high dosage of PCE is used in APs, which leads to noticeable changes in modulus curves, despite fluctuating data in the lower oscillation strain region. The critical strain of GB suspension generally corresponds to the end of the linear viscoelastic region or the onset of flow.[31,34] The sweep oscillation results are consistent with the yield stress results in Figure 4B, which suggests that a higher dosage of PCE in APs tends to result in poorly flowable GB suspension.

Figure 6E,F presents the comparison between the storage modulus (G') and loss modulus (G'') at the dosage of PCE (0.20%) made by KCl solutions at 3 and 180 mM. For the results at a lower ionic strength (3 mM), the PCE did not change storage modulus (G') and loss modulus (G'') greatly at various resting times. At higher ion strength (180 mM), both the moduli (G' and G'') curves gradually shifted to the right with resting time, and the plateau of storage modulus (G') at 120 min was found to be at approximately 10^2 Pa, which is 10 times higher than that of the sample (about 10 Pa) at 0 min. As shown in Figure 6G,H, a similar trend was observed: a more pronounced difference in modulus curves at various resting times at a higher ionic strength (180 mM). Between the resting times of 0 and 120 min, almost a hundred times difference was found for the plateau of storage modulus of the sample with 180 mM $CaCl_2$ and 0.20% PCE.

The results in sweep oscillation experiments show good agreement with yield stress over resting time, as depicted in Figure 4–6. The rheological results over time raise an essential question of why in a relatively inert system, that is, GB suspension, the higher dosage of PCE in APs and identical PCE dosage in high ionic strength (KCl and $CaCl_2$ solution) leads to a continuously increased yield stress over resting time. It is widely accepted that factors, including surface electrochemical characteristics, adsorption on the surface of particles, and PCE morphology, could all be possible reasons for the change in rheological properties.[3–5,16] Therefore, various characterizations of the GB suspension in this study were conducted to reveal the mechanism of variation in the rheological performance over resting time.

3.2 | Zeta potentials

We first investigate the surface charge properties of the GB suspension at various resting times, and zeta potential results are summarized in Figure 7. It can be seen that the zeta potentials are negative, which suggests an in total negatively charged surface of the GBs. The zeta potentials could be up to –160 mV when ionic strength is low to 0 and 3 mM, and a similar range of zeta potentials can also be found in nano-particles[35] and mica[36] in aqueous solution when fewer ions are present.

In Figure 7A, it is seen that the increase in PCE dosage (<0.10%) in an APs-made sample will first reduce the absolute zeta potentials (may relate to hydrogen ions [H^+] from the PCE) and then the absolute zeta potentials are gradually increased as a function of PCE dosage. In the KCl and $CaCl_2$ solution-made GB suspensions, increasing ionic strength from 0 to 180 mM gradually reduced the zeta potentials. In all the cases, after 60 and 120 min of resting, higher absolute values for zeta potentials (more negative) are observed compared to the sample at 0 min, implying an increased electrostatic repulsion force among particles after resting, which will be discussed in Section 4.1.

3.3 | PCE adsorption in GB suspension

Figure 8 shows the amount of PCE adsorbed by the GB suspension. It is seen from Figure 8A that in the APs prepared with GB suspension, the increase in PCE dosage will lead to a higher PCE adsorption on the surface of GB particle. At PCE dosage of 0.20% or lower, there is no prominent effect of the resting time on the adsorption behavior. However, when 0.4% PCE is added after 120 min of rest, a noticeable increase in the amount of PCE adsorbed from 2.0 to 2.8 mg/g by GB weight is found. For the KCl and $CaCl_2$ solution-made samples, it is found that initially (0 min), the strength of the ion from 0 to 180 mM increase will lead to more PCE adsorbed amount, especially for the KCl solution-made GB suspension. After 60 and 120 min resting, the PCE adsorption amount is increased to a certain degree, especially when the ionic strength is high. At the same ionic strength (180 mM), the PCE adsorption increase amount in the $CaCl_2$-made sample is higher than that of the KCl-made sample.

3.4 | DLS measurement

The effect of PCE dosage and ionic strength (from KCl and $CaCl_2$) on the relative hydrodynamic radius of PCE molecules was studied by DLS. In the presence of a high concentration of ions, the change in hydrodynamic radius

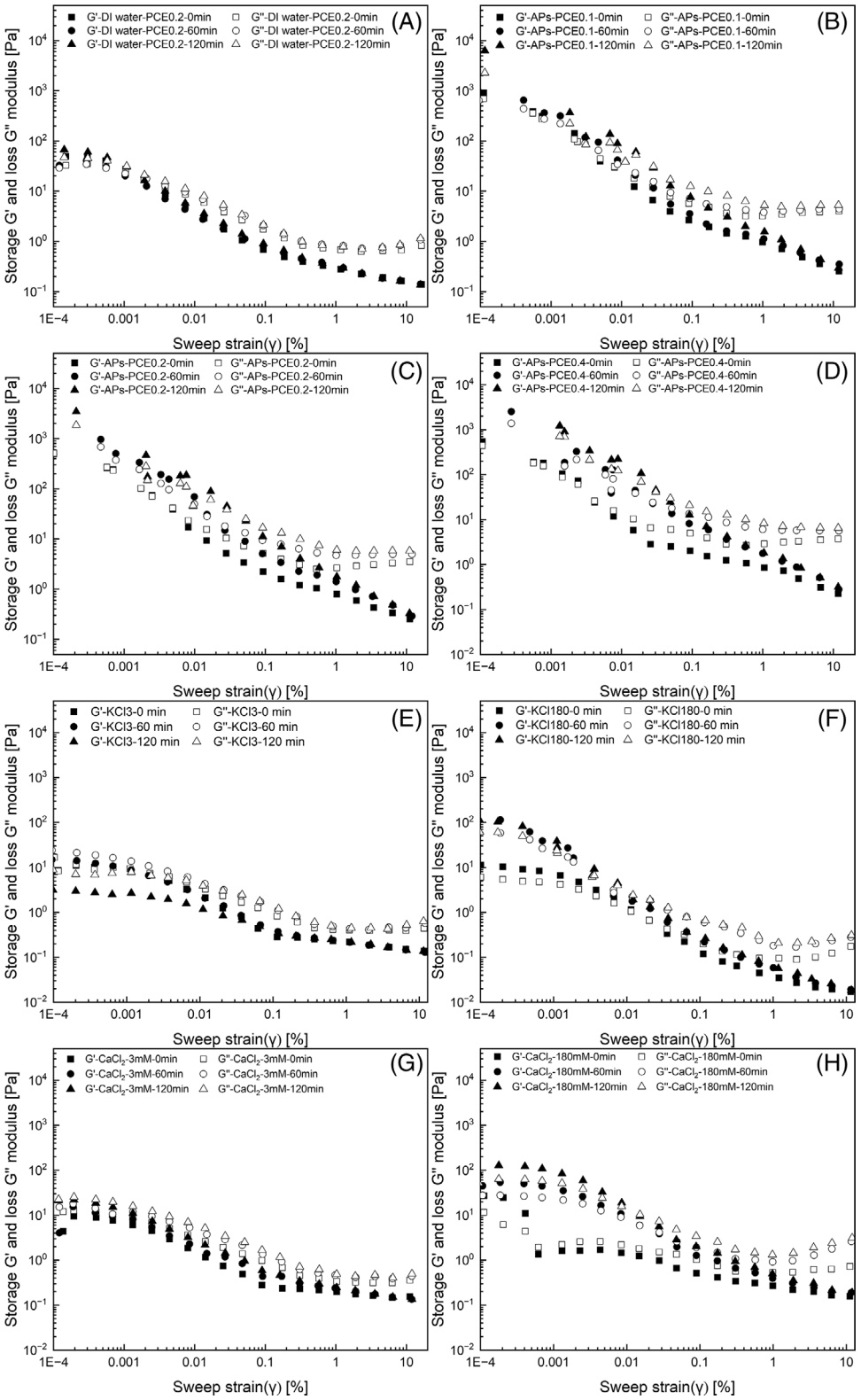

FIGURE 6 Storage modulus (G') and loss modulus (G'') as a function of sweep strain at 0, 60, and 120 min for selected glass bead (GB) suspensions made of deionized (DI) water with polycarboxylate superplasticizer (PCE)-0.2% (A), the artificial pore solution (APs) with PCE-0.1% (B), the APs with PCE-0.2% (C), APs with PCE-0.4% (D), KCl solution at 3 mM with PCE-0.2% (E), KCl solution at 180 mM with PCE-0.2% (F), $CaCl_2$ solution at 3 mM with PCE-0.2% (G), and $CaCl_2$ solution at 180 mM with PCE-0.2% (H).

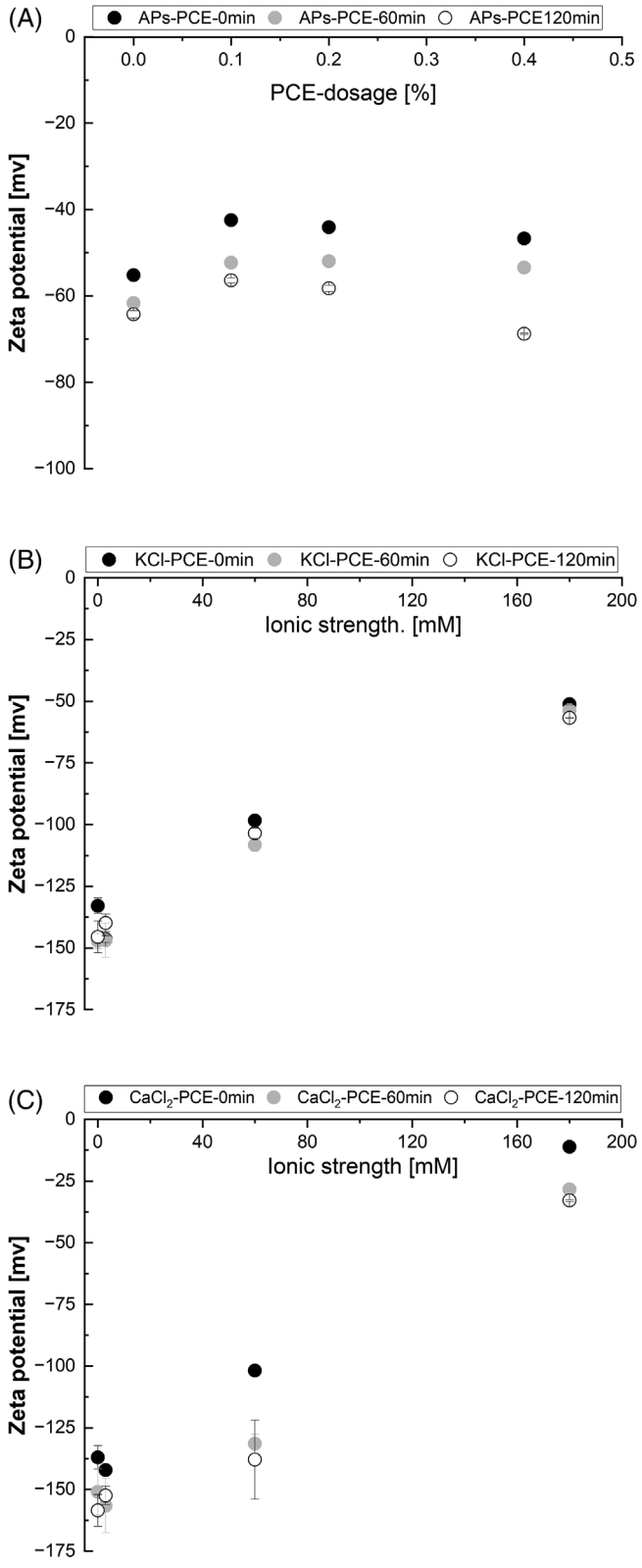

FIGURE 7 Zeta potential values for the artificial pore solution made of glass bead (GB) suspension as a function of polycarboxylate superplasticizer (PCE) dosage (A) and ionic strength (KCl solution (B) and $CaCl_2$ solution (C)) at 0, 60, and 120 min. Note the different scales for (A), (B), and (C). APs, artificial pore solution.

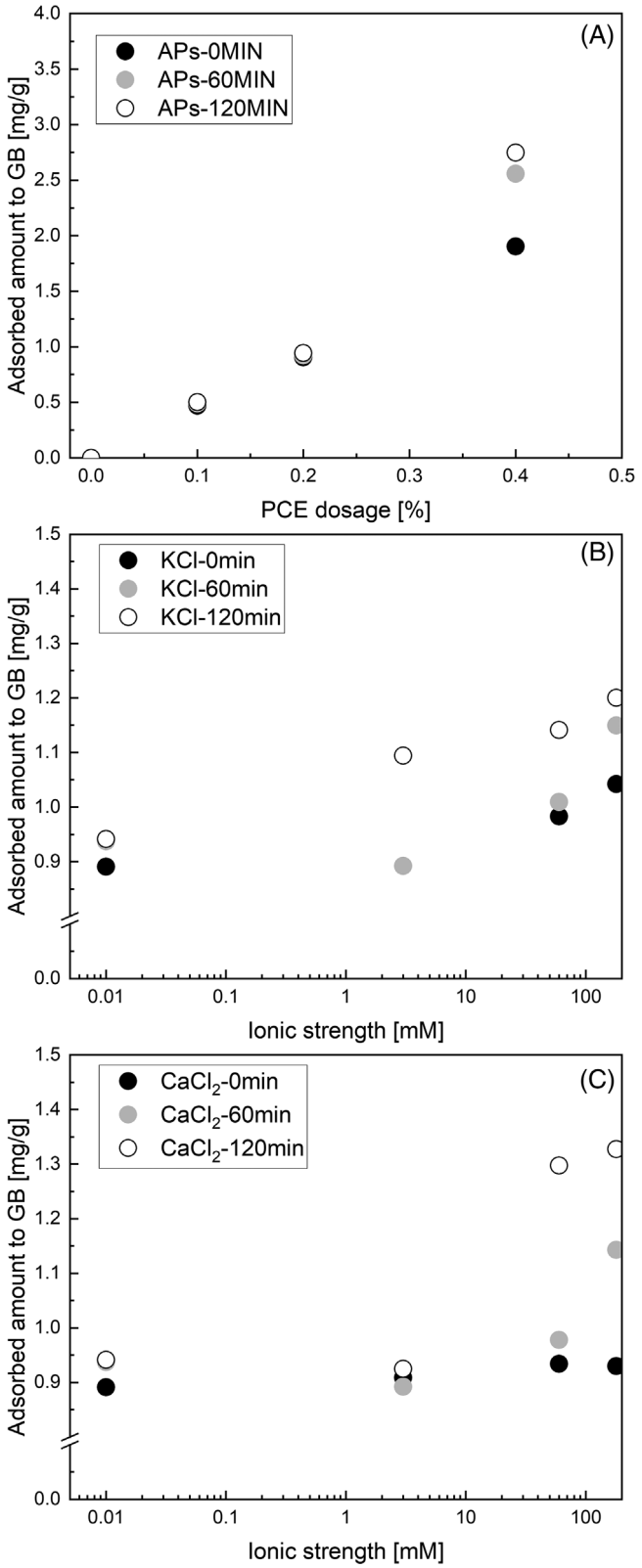

FIGURE 8 Adsorbed amount of the artificial pore solution made of glass bead (GB) suspension as a function of polycarboxylate superplasticizer (PCE) dosage (A) and ionic strength (KCl solution (B) and $CaCl_2$ solution (C)) at 0, 60, and 120 min.

of PCE molecules is highly dependent on the resting time, as shown in Figure 9. To be specific, Figure 9A illustrates that the PCE in DI water did not change over resting time. However, in APs, the relative hydrodynamic radius could be up to seven to six times bigger than that in the sample at 0 min.

In Figure 9B,C, it is observed that the ionic strength increase contributed to a higher hydrodynamic diameter of PCE molecules. The PCE at an ionic strength of 180 mM of $CaCl_2$ solution is about 3.5 times bigger (than that of the sample at 0 min), which is even greater than that of the solutions made by KCl solution with ionic strength of 180 mM. This observation suggests that the cross-linking effects between PCE molecules were enhanced by Ca^{2+} ions in the solution. In fact, the PCE in the ionic solution can get bigger spontaneously and the additional mixing of the PCE in the ionic solution can get it even bigger, as shown in Figure S1. In addition, the radius of PCE in solutions measured at 0 min by DLS is summarized in Table S1.

4 | ANALYSIS AND DISCUSSION

4.1 | Zeta potential and PCE adsorption

The zeta potential is dependent on the surface charges of the particle, in which more OH^- will help the dissociation of silanol groups from the uncharged group (SiOH) to the negatively charged group (SiO^-).[37,38]

$$SiOH + OH^- = SiO^- + H_2O \quad (3)$$

If more cations are in the solution, SiO^- may adsorb cations from the pore solution to get more sites on the surface to be positively charged. The increase in ionic strength in $CaCl_2$ and KCl solutions leads to higher cation adsorption by GBs, which explains the decrease in zeta potential (absolute values) as a function of ionic strength in Figure 7. It is noted that PCE can only be adsorbed on a positively charged site by their –COO– group on the backbone.[39–41] That is why with more ions present in the pore solution, a more significant PCE adsorption can be found in Figure 8B,C.

The total ionic strength in the sample with APs is up to 386 mM, resulting in sufficient positively charged sites at the surfaces for PCE adsorption. This could be the origin of the increased values of zeta potential and enhanced adsorption as a function of PCE dosage in Figures 7A and 8A. Moreover, the Debye length ($\lambda_D = \kappa^{-1}$) is related to the electrostatic effect in a solution, which can be described

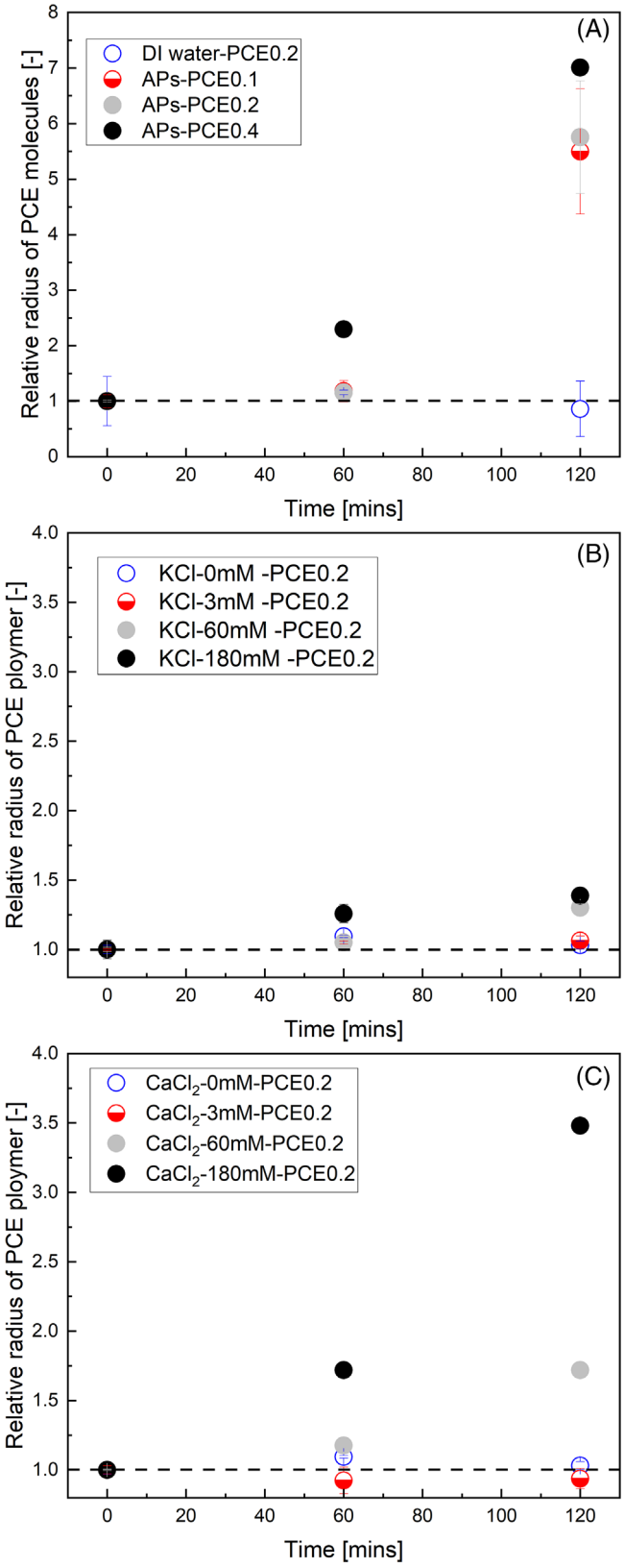

FIGURE 9 Relative hydrodynamic diameter of polycarboxylate superplasticizer (PCE) molecules in the artificial pore solution (A), KCl solution (B), and $CaCl_2$ solution (C) (PCE dosage is 0.20%) as a function of resting time from 0 to 120 min. APs, artificial pore solution; DI water, deionized water.

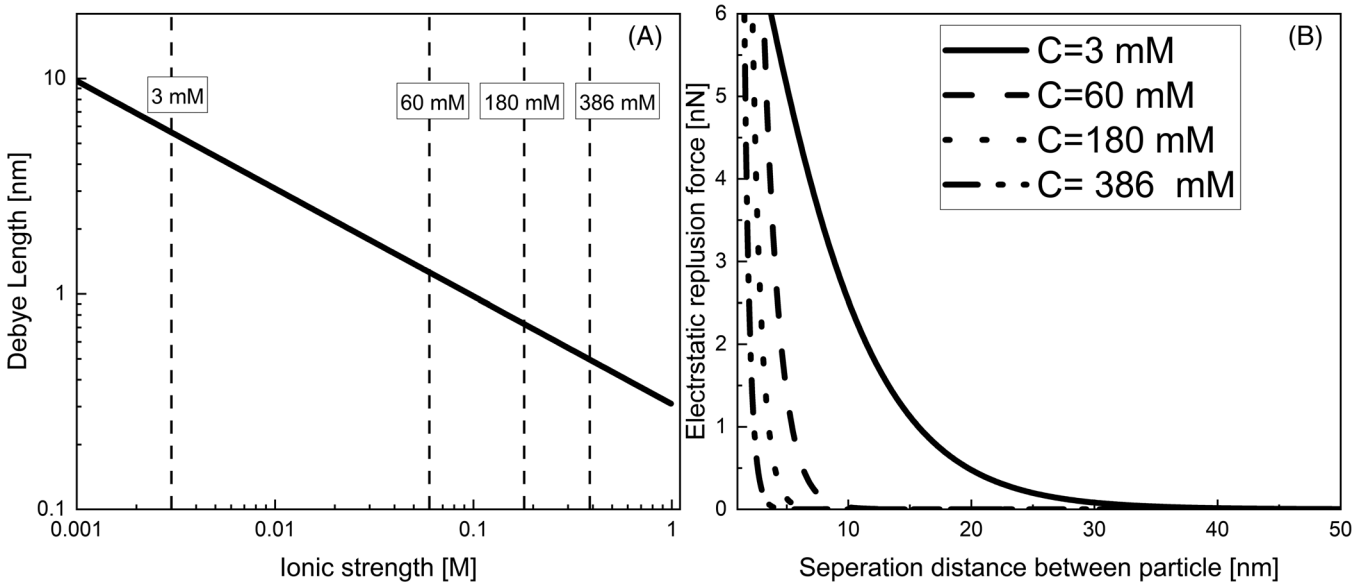

FIGURE 10 The Debye length of glass beads in solution with various ionic strengths (A) and the electrostatic repulsion force as a function of the distance between particles (B).

by Equation (4).

$$\kappa^{-1} = \sqrt{\frac{\varepsilon_r \varepsilon_0 k_B T}{2 e_c^2 I}} \tag{4}$$

where I is the ionic strength of the solution in the unit of number/m^3, ε_0 is the permittivity of free space, ε_r is the dielectric constant, k_B is the Boltzmann constant, T is the absolute temperature in Kelvin, and e_c is the elementary charge (1.602×10^{-19} C). More ions in the pore solution will suppress the Debye length by the shielding effect (electrically screened).[42,43] The computed Debye length as a function of ionic strength is plotted in Figure 10A. The electrostatic force can be estimated by Equation (5), according to Refs.16, 41

$$F_e = 2\pi\varepsilon\varepsilon_0\psi^2 d\frac{\kappa e^{-\kappa h}}{1+e^{-\kappa h}} \tag{5}$$

where ψ is the surface charge (positively related to the absolute value of zeta potential,[41,42] here, the zeta potential is denoted as ψ), and d is the particle size of GBs. The electrostatic force as a function of distance is shown in Figure 10B, in which the range of the electrostatic repulsion force decreases with increasing ionic strength from 3 to 386 mM. Thus, higher ionic strength at 0 min contributes to the higher yield stress in Figures 4 and 5.

However, after resting times of 60 and 120 min, zeta potential values of the GB suspensions in Figure 7A are found to be even bigger (resulting from surface dissociation by OH^-), implying a weaker adhesion force among GB particles according to Equation (5). This is consistent with the interparticle force measurement by atomic force microscopy (AFM) as shown in Figure S2, in which a greater repulsion force between two GBs (in KCl solution with or without PCE) can be observed during resting. Except for intermediate ion concentration which showed no uniform behavior with resting time. Besides, the enhanced PCE adsorption after 60 and 120 min of rest (see Figure 8) means that more PCE can disperse GB particles by the steric hindrance.[9] The greater electrostatic force and enhanced adsorption, in general, means less force is needed for the movement of particles, which contradicts the higher yield stress found in this study.

4.2 | PCE size change in the aqueous phase and its possible impacts on rheology

The results in Figure 9 indicated that the size of PCE in solution becomes bigger as a function of resting time, especially when a high ionic strength solution is used. The increase in PCE size could be due to the entanglement among them being enhanced by the cross-linking effect between the –COO– group and cations. As a result, several PCE molecules are bound together, contributing to a higher hydrodynamic radius of PCE. The Ca^{2+} ion has a larger radius (0.99 Å) than K^+ ions.[44] In three-dimensional space, the groups (i.e., $-COO^-$) of polymers binding to a smaller size of ions (i.e., K^+) should be at a closer distance. This spatial arrangement will enhance steric hindrance[45,46] between the bound polymers and unbound polymers, which may reduce the probability of the ion–polymer bonding compared to that in the case of bigger sizes of ions (i.e., Ca^{2+}). Therefore, greater changes

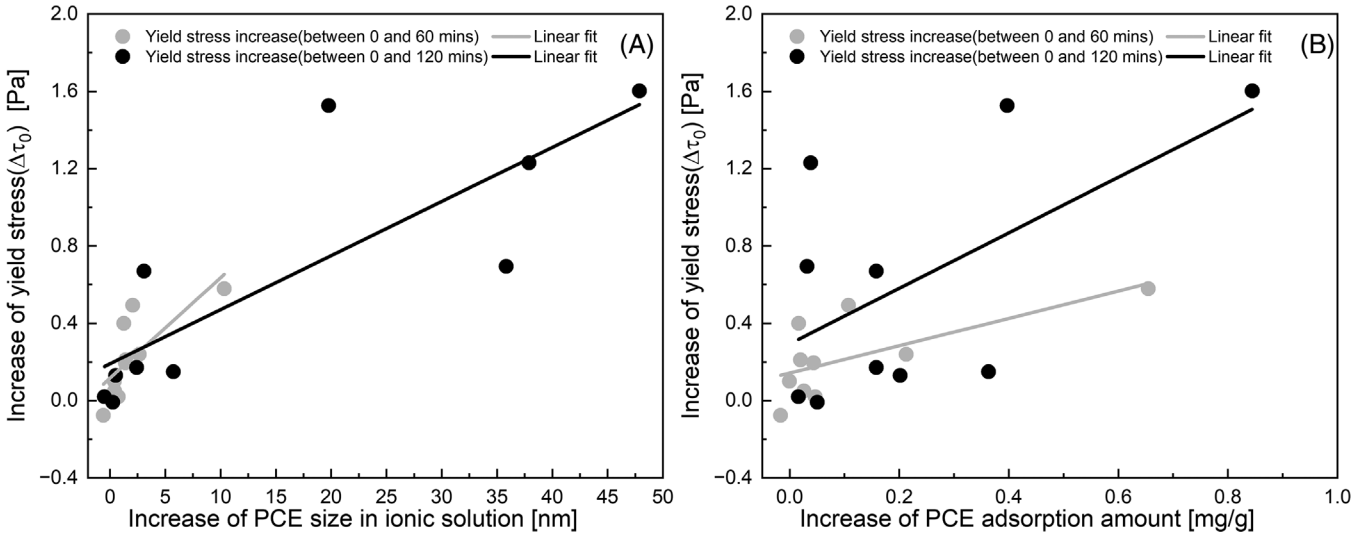

FIGURE 11 Relationship between the increase in yield stress ($\Delta\tau_0$) and increase in relative polycarboxylate superplasticizer (PCE) size (A) as measured by dynamic light scattering as well as the increase in PCE adsorption (B) on glass beads.

have been found in the PCE radius in the presence of Ca^{2+} ions rather than K^+ ions, as shown in Figure 9B,C. The increased size of the free PCE in the sample could have multiple effects on rheological properties. In this study, we mainly discuss the impact of the bridging effect and depletion force due to the variation in PCE size as a function of resting time.

4.2.1 | Bridging effect

The bridging effect is related to the size of the polymer (molecular weight)[47] and the affinity of the polymer chain[48] to the surface. In the study of Brumaud et al.,[47] the cellulose ethers with R_g ranging from 18 to 73 nm could bridge the cement grains and contribute to the increase in the yield stress. Here, we plot in Figure 11 the increase in the yield stress ($\Delta\tau_0$) and the size difference of PCE (Figure 11A) measured at the different resting times by DLS, as well as the adsorbed amount of PCE (Figure 11B).

It can be seen that the PCE molecule size and the increase in yield stress (compared to the values measured at the resting time of 0 min) are positively correlated, which suggests that the bridging effect may be enhanced by the increased size of PCE and then lead to higher yield stress. In our study, the initial radius of gyration (R_g) for the PCE was estimated by an empirical formula ($R_g = 0.032556 \times M_w^{0.537\,nm}$) established in the previous research,[49,50] which gives a value of 7.97 nm for PCE used in this study. As a function of time, this radius could be up to seven times bigger (in APs) than its initial size, which makes it possible for the PCE in solution to bind the GB particles. The increased number of cations, such as Ca^{2+} and K^+, would enhance the affinity of the enlarged PCE because of complexation with the surface of GBs which may also enhance the bridging effect. As shown in Figure 11B, the increase in the amount of PCE adsorbed positively correlates with the yield stress increase, which suggests that PCE adsorption in the latter stage, 1 or 2 h contributes to increasing yield stress rather than reducing it. Combining the analysis from Figure 11A,B, it can be inferred that the PCE with a bigger size (caused by ion–polymer interactions) adsorbed on GBs may not disperse the particles but tends to bridge them.

Besides, the solid content for the GB suspension is up to 64.0%, and the unavoidable sedimentation during resting time results in a small interparticle space. Thus, the sedimentation may facilitate the enlarged PCE coils to bridge the GB particles to form aggregates, even though there is an additional 30 s of mixing at different resting times before the rheological measurements. In addition, in our study, we found that the amount of macro-agglomerates (calculated as an area ratio of agglomerates) decreased as a function of resting time, as measured by optical microscopy and image analysis, as shown in Figures S3 and S4, which may result from the agglomerate destruction by mixing. Thus, if the bridging effect caused by the enlarged size of PCE polymers does exist among the GB particles, it may bridge GB particles at the microscale (micron level) rather than the macroscale (millimeter level).

4.2.2 | Depletion force

Another possible explanation for the increased yield stress over resting time is the increase in the attractive force of

depletion. In this study, 30%–50% of PCE polymers are not fixed to the GB surface after mixing (0 min), as shown in the adsorption measurement (Figure 8). These non-adsorbed PCE polymers in solution would contribute to the depletion force among particles. The depletion is an entropy force that emphasizes the phenomenon created by the free polymer in a region of pure solvent between particles,[16] leading to an appearance of osmotic pressure pushing particles closer. Principally, two regimes define the depletion force among the particle, dilute and semi-dilute regimes,[16,24] depending on the critical overlapping concentration for PCE (c^*).

$$c^* = \frac{M_w}{N_A R_g^3} \tag{6}$$

where N_A is the Avogadro constant (6.022×10^{23}), R_g at 0 min equals 7.97 nm (based on the empirical formula[49]), and M_w of PCE is 28 090 g/mol, so the c^* for PCE is estimated to be 0.092 g/g of water. In this study, the highest PCE dosage used is 0.40% by GB weight, which gives the concentration of 0.015 g/g by water (water-to-glass ratio = 0.26). Except for the PCE adsorption, the PCE in GB suspension is considered a dilute regime, in which polymer coils in the solvent are considered far from one another. The depletion force for the diluted regime can be described as follows[16]:

$$F_{d,t} = 0 \quad \text{If } h > 2\bar{R}_{g,0} \tag{7}$$

$$F_{d,t} = -\rho_{s,t} k_B T \pi d_{GB} (2\bar{R}_{g,0} - h) \quad \text{If } h < 2\bar{R}_{g,0} \tag{8}$$

where $\rho_{s,t}$ is the number density of free PCEs (single polymer case) in the bulk solution at 0. The $\rho_{s,t}$ depends on the PCE dosage and the adsorbed amount in the sample at different resting times, d_{GB} is the mean diameter of the GBs (9.13 μm), k_B is the Boltzmann constant (1.38×10^{-23} J/K), T is the absolute temperature (295 K), and $\bar{R}_{g,0}$ is the mean hydrodynamic radius of the non-adsorbed PCE at zero time.

It is noted that the PCE polymer gets enlarged as a function of time when high ionic strength or a high PCE dosage is applied, as shown in Figure 10. The enlarged size of PCE means the depletion force will influence the particles at a longer range according to Equation (8). If we assume here that the bonding between the PCE molecules (possibly resulting from cations such as Ca^{2+} and K^+) has no radius loss (the size of the bonded PCE coil equals to the sum of the individual size), the average radius of PCE ($\bar{R}_{g,t}$) at time t can be expressed as:

$$\bar{R}_{g,t} = \frac{\bar{R}_{g,0}}{1 - \phi(t)} \tag{9}$$

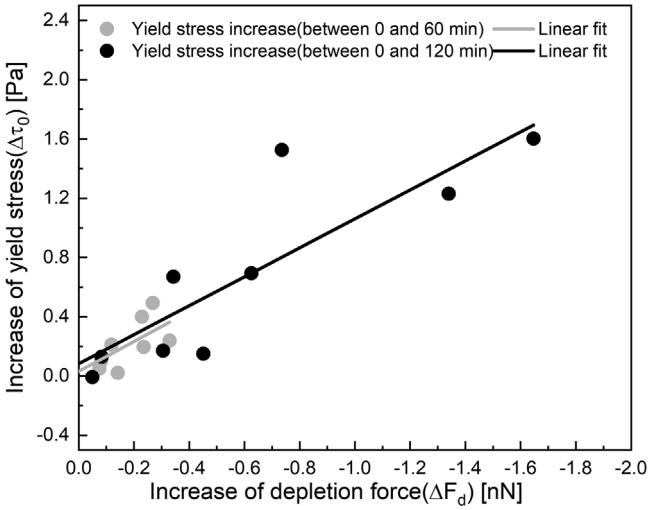

FIGURE 12 Relationship between the increase in yield stress ($\Delta\tau_0$) and difference of depletion force at $h = 2\bar{R}_{g,0}$ as calculated by Equation (12).

where $\phi(t)$ is the fraction of amount of non-adsorbed, bonded PCE molecule pairs to total amount of non-adsorbed PCE molecules. At $t = 0$, we assume that there is no binding among PCE polymers; thus, $\phi(0) = 0$. It can be inferred that this bonding among PCE molecules not only increases the size of PCE but also decreases the number density of PCE in the bulk solution. Hence, the number density of PCEs (considering the bonding effect among PCE polymers) in the bulk solution can be described as:

$$\rho_{b,t} = \rho_{s,t}(1 - \phi(t)) \tag{10}$$

Based on Equation (8), the depletion force at the resting time of t can be rewritten as Equation (11):

$$F_{d,t} = -\rho_{s,t}(1 - \phi(t)) k_B T \pi d_{GB} (2\bar{R}_{g,t} - h) \tag{11}$$

If we only look at the depletion force at a separation distance of $h = 2\bar{R}_{g,0}$,then $F_{d,0} = 0$ and the depletion force difference between time t and 0, can be computed by Equation (12).

$$\Delta F_d = F_{d,t} - F_{d,0} = -2\rho_{s,t} k_B T \pi d_{GB} \bar{R}_{g,0} \left(1 - \frac{\bar{R}_{g,0}}{\bar{R}_{g,t}}\right) \tag{12}$$

As shown in Refs.,[16, 51] the rheological properties (i.e., yield stress) directly relate to the variation in the interparticle force when solid content is fixed. Here, in this study, we analyze the relationship between the yield stress difference ($\Delta\tau_0$) compared to the resting time of 0 min, ΔF_d, and the relative increase in depletion force at $h = 2\bar{R}_{g,0}$ and the analysis results are given in Figure 12.

Figure 12 shows that, generally, the increase in depletion force (ΔF_d) positively correlated with the yield stress difference at resting times of 60 and 120 min compared to that at 0 min. The dependency between the two values is not very significant, in which the correlation coefficients (R^2) at 60 and 120 min are 0.05 and 0.56, respectively. The results suggest that the extended range and increased amplitude of depletion force caused by the PCE size change could be the origin of the increase in yield stress over resting time.

The calculation of the depletion force includes multiple variables, $\rho_{b,t}$ and $\Phi(t)$, which relate to the PCE adsorption and hydrodynamic radius results. In this regard, the calculation of the depletion force could be influenced by the accuracy of TOC and DLS measurements, which may affect the correction between the depletion attractive force and yield stress. In addition, the depletion force is calculated at a fixed distance $h = 2\bar{R}_{g,0}$ between particles, and the initial hydrodynamic radius ($\bar{R}_{g,0}$) used for calculation is a theoretical value. The oversimplification of R_g at 0 min may also impact the dependency between the two values. The relative hydrodynamic radius is measured without the GBs present in the solution. This case is also not the reality that PCE and ions in the system will face, which may also affect the analysis results above. Yet, obtained results provided a reliable model of the influence of the resting time on the rheological behavior induced by PCE, which could be used for practical engineering.

5 | CONCLUSION

In this paper, we studied the rheological properties of GB suspension prepared with various PCE dosages and ionic strength solutions as a function of resting time. The shear yield stress and sweep oscillation measurement were jointly employed to evaluate rheological behavior.

Our results indicate that the yield stress increases with time when high dosages of PCE in APs or identical PCE dosages in high ionic strength solutions are applied. The results from strain sweep experiments are in good agreement with the yield stress over time. The surfaces of GBs are negatively charged, and increasing ionic strength reduces the absolute value of zeta potentials, while more PCE in solutions increases it. This is a strong hint for the adsorption of PCE at the surfaces of the GBs. The zeta potential increases to a certain degree after resting, implying higher electrostatic repulsion force, which contradicts the increased yield stress over time. The results confirm that the PCE adsorption is enhanced with time, suggesting that the PCE on surfaces in the latter stages tends to bridge the particles rather than disperse them. The hydrodynamic radius of PCE increases with resting time, and the calculated depletion forces resulting from non-adsorbed PCE size change increase with yield stress. This paper highlights the variation in the depletion force and bridging effect over time resulting from PCE size change and its impacts on rheological properties, which has been overlooked in previous studies and practices.

ACKNOWLEDGMENTS

The authors gratefully thank the German Research Foundation (DFG) for funding the Priority Program DFG SPP 2005 Priority Program "Opus Fluidum Futurum—Rheology of Reactive, Multi-Scale, Multiphase Construction Materials" (project number 387092747) and BASF for providing the polycarboxylate superplasticizer samples. In addition, the authors would like to deeply appreciate the assistance from Jessica Conrad, Halim Choo, and Dr. Christian Lehmann at Technische Universität Berlin and Kun Zhang in Bundesanstalt für Materialforschung und prüfung (BAM) for performing the experiments.

Open access funding enabled and organized by Projekt DEAL.

ORCID

Yanliang Ji https://orcid.org/0000-0002-7051-4440
Zichen Lu https://orcid.org/0000-0001-5794-3382
Dietmar Stephan https://orcid.org/0000-0002-1893-6785

REFERENCES

1. Roussel N, Bessaies-Bey H, Kawashima S, Marchon D, Vasilic K, Wolfs R. Recent advances on yield stress and elasticity of fresh cement-based materials. Cem Concr Res. 2019;124:105798. https://doi.org/10.1016/j.cemconres.2019.105798
2. Wallevik OH, Wallevik JE. Rheology as a tool in concrete science: the use of rheographs and workability boxes. Cem Concr Res. 2011, 41(12):1279–88. https://doi.org/10.1016/j.cemconres.2011.01.009
3. Roussel N. Rheological requirements for printable concretes. Cem Concr Res. 2018;112:76–85. https://doi.org/10.1016/j.cemconres.2018.04.005
4. Biricik Ö, Mardani A. Parameters affecting thixotropic behavior of self compacting concrete and 3D printable concrete; a state-of-the-art review. Constr Build Mater. 2022;339:127688. https://doi.org/10.1016/j.conbuildmat.2022.127688
5. Marchon D, Kawashima S, Bessaies-Bey H, Mantellato S, Ng S. Hydration and rheology control of concrete for digital fabrication: potential admixtures and cement chemistry. Cem Concr Res. 2018;112:96–110. https://doi.org/10.1016/j.cemconres.2018.05.014
6. Jones SZ, Hipp JB, Allen AJ, Gagnon C V. Rheology and microstructure development of hydrating tricalcium silicate—implications for additive manufacturing in construction. Cem Concr Res. 2022;152:106651. https://doi.org/10.1016/j.cemconres.2021.106651
7. Bogner A, Link J, Baum M, Mahlbacher M, Gil-Diaz T, Lützenkirchen J, et al. Early hydration and microstructure formation of Portland cement paste studied by oscillation rheology, isothermal calorimetry, 1H NMR

relaxometry, conductance and SAXS. Cem Concr Res. 2020;130:105977. https://doi.org/10.1016/j.cemconres.2020.105977
8. Ley-Hernández AM, Feys D. Resting time effect on the rheological behavior of cement paste in presence of superplasticizer. Cem Concr Res. 2021;142:106347. https://doi.org/10.1016/j.cemconres.2020.106347
9. Plank J, Sakai E, Miao CW, Yu C, Hong JX. Chemical admixtures—chemistry, applications and their impact on concrete microstructure and durability. Cem Concr Res. 2015;78:81–99. https://doi.org/10.1016/j.cemconres.2015.05.016
10. Bessaies-Bey H, Baumann R, Schmitz M, Radler M, Roussel N. Organic admixtures and cement particles: competitive adsorption and its macroscopic rheological consequences. Cem Concr Res. 2016;80:1–9. https://doi.org/10.1016/j.cemconres.2015.10.010
11. Petit J-Y, Khayat KH, Wirquin E. Coupled effect of time and temperature on variations of plastic viscosity of highly flowable mortar. Cem Concr Res. 2009;39(3):165–70. https://doi.org/10.1016/j.cemconres.2008.12.007
12. Adjou N, Yahia A, Oudjit MN, Dupuis M. Influence of HRWR molecular weight and polydispersity on rheology and compressive strength of high-performance cement paste. Constr Build Mater. 2022;327:126980. https://doi.org/10.1016/j.conbuildmat.2022.126980
13. Bauchkar SD, Chore HS. Effect of PCE superplasticizers on rheological and strength properties of high strength self-consolidating concrete. Adv Concr Construct. 2018;6(6):561–83. https://doi.org/10.12989/acc.2018.6.6.561
14. Schmidt W, Brouwers HJH, Kühne H-C, Meng B. Influences of superplasticizer modification and mixture composition on the performance of self-compacting concrete at varied ambient temperatures. Cem Concr Compos. 2014;49:111–26. https://doi.org/10.1016/j.cemconcomp.2013.12.004
15. Lei L, Plank J. A concept for a polycarboxylate superplasticizer possessing enhanced clay tolerance. Cem Concr Res. 2012;42(10):1299–306. https://doi.org/10.1016/j.cemconres.2012.07.001
16. Bessaies-Bey H, Palacios M, Pustovgar E, Hanafi M, Baumann R, Flatt RJ, et al. Non-adsorbing polymers and yield stress of cement paste: effect of depletion forces. Cem Concr Res. 2018;111:209–17. https://doi.org/10.1016/j.cemconres.2018.05.004
17. Arshad M, Easa A, Qiblawey H, Nasser M, Benamor A, Bhosale R, et al. Experimental measurements and modelling of viscosity and density of calcium and potassium chlorides ternary solutions. Sci Rep. 2020;10(1):16312. https://doi.org/10.1038/s41598-020-73484-4
18. Martínez JM, Pappalardo RR, Sánchez Marcos E. First-principles ion−water interaction potentials for highly charged monatomic cations. computer simulations of Al^{3+}, Mg^{2+}, and Be^{2+} in water. J Am Chem Soc. 1999;121(13):3175–84. https://doi.org/10.1021/ja9830748
19. Zhang HL, Chen GH, Han SJ. Viscosity and density of H_2O+NaCl+$CaCl_2$ and H_2O+KCl+$CaCl_2$ at 298.15 K. J Chem Eng Data. 1997;42(3):526–30. https://doi.org/10.1021/je9602733
20. Krieger IM, Dougherty TJ. A mechanism for non-Newtonian flow in suspensions of rigid spheres. Trans Soc Rheol. 1959;3(1):137–52. https://doi.org/10.1122/1.548848
21. Bird RB, Stewart WE. Transport phenomena. 2nd ed. John Wiley & Sons, Inc; 2007.
22. Choi W, Mahajan U, Lee S-M, Abiade J, Singh RK. Effect of slurry ionic salts at dielectric silica CMP. J Electrochem Soc. 2004;151(3):185–89. https://doi.org/10.1149/1.1644609
23. Leroy P, Tournassat C, Bernard O, Devau N, Azaroual M. The electrophoretic mobility of montmorillonite. Zeta potential and surface conductivity effects. J Colloid Interface Sci. 2015;451:21–39. https://doi.org/10.1016/j.jcis.2015.03.047
24. Feigin RI, Napper DH. Depletion stabilization and depletion flocculation. J Colloid Interface Sci. 1980;75(2):525–41. https://doi.org/10.1016/0021-9797(80)90475-0
25. Schmidt W, Weba L. Influences of hydration effects on the flow phenomena of concrete with admixtures. Materials and value chains for sustainable, inclusive, and resilient urbanisation in Africa view project. Dar es Salaam, Tanzania; 2016. p. 79–88.
26. Tian H, Kong X, Miao X, Jiang L, Pang X. A new insight into the working mechanism of PCE emphasizing the interaction between PCE and Ca^{2+} in fresh cement paste. Constr Build Mater. 2021;275:122133. https://doi.org/10.1016/j.conbuildmat.2020.122133
27. Lu Z, Liu S, Stephan D. Effects of cations on the yield stress of a highly concentrated suspension of glass beads with the addition of polycarboxylate superplasticizer. Colloids Surf A Physicochem Eng Asp. 2019;575:176–83. https://doi.org/10.1016/j.colsurfa.2019.05.015
28. Bessaies-Bey H, Baumann R, Schmitz M, Radler M, Roussel N. Effect of polyacrylamide on rheology of fresh cement pastes. Cem Concr Res. 2015;76:98–106. https://doi.org/10.1016/j.cemconres.2015.05.012
29. Lange A, Hirata T, Plank J. The role of non-adsorbed PCE molecules in cement dispersion: experimental evidence for a new dispersion mechanism. SP-288: Tenth International Conference on Superplasticizers and other Chemical Admixtures. Vol 288. American Concrete Institute; 2012. p. 1–15. https://doi.org/10.14359/51684246
30. Lei L, Chomyn C, Schmid M, Plank J. Characterization data of reference industrial polycarboxylate superplasticizers used within Priority Program DFG SPP 2005 “Opus Fluidum Futurum—Rheology of reactive, multiscale, multiphase construction materials.” Data Brief. 2020;31:106026. https://doi.org/10.1016/j.dib.2020.106026
31. Jiao D, Lesage K, Yardimci MY, El Cheikh K, Shi C, De Schutter G. Rheological behavior of cement paste with nano-Fe_3O_4 under magnetic field: magneto-rheological responses and conceptual calculations. Cem Concr Compos. 2021;120:104035. https://doi.org/10.1016/j.cemconcomp.2021.104035
32. Pecora R. Dynamic light scattering: applications of photon correlation spectroscopy. Plenum Press; 1985. https://doi.org/10.1002/bbpc.19870910455
33. Washington C. Particle size analysis in pharmaceutics and other industries: theory and practice. Ellis Horwood; 1992. https://doi.org/10.1201/b12596
34. Betioli AM, Gleize PJP, Silva DA, John VM, Pileggi RG. Effect of HMEC on the consolidation of cement pastes: isothermal calorimetry versus oscillatory rheometry. Cem Concr Res. 2009;39(5):440–45. https://doi.org/10.1016/j.cemconres.2009.02.002

35. Jain K, Mehandzhiyski AY, Zozoulenko I, Wågberg L. PEDOT:PSS nano-particles in aqueous media: a comparative experimental and molecular dynamics study of particle size, morphology and z-potential. J Colloid Interface Sci. 2021;584:57–66. https://doi.org/10.1016/j.jcis.2020.09.070
36. Lameiras FS, de Souza AL, de Melo VAR, Nunes EHM, Braga ID. Measurement of the zeta potential of planar surfaces with a rotating disk. Mater Res. 2008;11(2):217–19. https://doi.org/10.1590/S1516-14392008000200018
37. Iler RK. The chemistry of silica. New York: Wiley; 1979.
38. Behrens SH, Grier DG. The charge of glass and silica surfaces. J Chem Phys. 2001;115(14):6716–21. https://doi.org/10.1063/1.1404988
39. Wu B, Chun B-W, Gu L, Kuhl TL. Adsorption properties of poly(carboxylate ether) to negatively charged surfaces in high-salt conditions. Cem Concr Res. 2019;118:102–10. https://doi.org/10.1016/j.cemconres.2019.02.003
40. Hommer H. Interaction of polycarboxylate ether with silica fume. J Eur Ceram Soc. 2009;29(10):1847–53. https://doi.org/10.1016/j.jeurceramsoc.2008.12.017
41. Li HC, De Bruyn PL. Electrokinetic and adsorption studies on quartz. Surf Sci. 1966;5(2):203–20. https://doi.org/10.1016/0039-6028(66)90082-3
42. Labbez C, Nonat A, Pochard I, Jönsson B. Experimental and theoretical evidence of overcharging of calcium silicate hydrate. J Colloid Interface Sci. 2007;309(2):303–7. https://doi.org/10.1016/j.jcis.2007.02.048
43. Lowke D, Gehlen C. The zeta potential of cement and additions in cementitious suspensions with high solid fraction. Cem Concr Res. 2017;95:195–204. https://doi.org/10.1016/j.cemconres.2017.02.016
44. Kinjo TG, Schnetkamp PPM. Ca^{2+} chemistry, storage and transport in biologic systems. Voltage-gated calcium channels. Boston, MA: Springer; 2000–2013. https://doi.org/10.1007/0-387-27526-6_1
45. Williams RJ. Calcium. Methods Mol Biol. 2002;172:21–49. https://doi.org/10.1385/1-59259-183-3:021
46. Williams RJ. Calcium: the developing role of its chemistry in biological evolution. In: Carafoli E, Klee C, editors. Calcium as a cellular regulator. New York: Oxford University Press, Inc.; 1999. p. 3–27.
47. Brumaud C, Baumann R, Schmitz M, Radler M, Roussel N. Cellulose ethers and yield stress of cement pastes. Cem Concr Res. 2014;55:14–21. https://doi.org/10.1016/j.cemconres.2013.06.013
48. Tadros TF. Dispersion of powders in liquids and stabilization of suspensions. Wiley; 2012. https://doi.org/10.1002/9783527656592
49. Fischer J, Paschek D, Geiger A, Sadowski G. Modeling of aqueous poly(oxyethylene) solutions. 2. Mesoscale simulations. J Phys Chem B. 2008;112(43):13561–71. https://doi.org/10.1021/jp805770q
50. Wang YW, Zhao HX, Shu X, Yang Y, Ran QP. Modelling the equilibrium sizes of comb-shaped MPEG-type polycarboxylate-type superplasticizers in dilute solution and their apparent molecular weight in conventional size exclusion chromatography. Acta Polym Sin. 2017;(6):1008–18. https://doi.org/10.11777/j.issn1000-3304.2017.16297
51. Flatt RJ, Bowen P. Yodel: a yield stress model for suspensions. J Am Ceram Soc. 2006;89(4):1244–56. https://doi.org/10.1111/j.1551-2916.2005.00888.x

SUPPORTING INFORMATION

Additional supporting information can be found online in the Supporting Information section at the end of this article.

How to cite this article: Ji Y, Becker S, Lu Z, Mezhov A, von Klitzing R, Wolfram S, et al. Effect of resting time on rheological properties of glass bead suspensions: Depletion and bridging force among particles. J Am Ceram Soc. 2024;107:624–639. https://doi.org/10.1111/jace.19469